Journal of Immunology and Regenerative Medicine 3 (2019) 13–25

Contents lists available at ScienceDirect

Journal of Immunology and Regenerative Medicine

journal homepage: www.elsevier.com/locate/regen

Comparison of the host macrophage response to synthetic and biologic surgical meshes used for ventral hernia repair

Catalina Pineda Molina[a,b], Ross Giglio[a,b], Riddhi M. Gandhi[a,b], Brian M. Sicari[a,c], Ricardo Londono[a], George S. Hussey[a,c], Joseph G. Bartolacci[a,b], Lina M. Quijano Luque[a], Madeline C. Cramer[a,b], Jenna L. Dziki[a,c], Peter M. Crapo[d], Stephen F. Badylak[a,b,c,*]

[a] McGowan Institute for Regenerative Medicine, University of Pittsburgh, Pittsburgh, PA, USA
[b] Department of Bioengineering, University of Pittsburgh, Pittsburgh, PA, USA
[c] Department of Surgery, University of Pittsburgh, Pittsburgh, PA, USA
[d] BDI Surgical, Becton, Dickinson and Company, Warwick, RI, USA

ARTICLE INFO

Keywords:
Biologic material
Degradable material
Host response
Macrophage phenotype
Surgical mesh
Synthetic material
Ventral hernia repair

ABSTRACT

The host innate immune response to a surgical mesh is arguably the most important determinant of tissue remodeling and functional outcome. Macrophage phenotype and the associated secretion of pro-inflammatory or anti-inflammatory cytokines during the first 10–14 days following implantation has been strongly associated with downstream events such as chronic inflammation vs. functional tissue remodeling, respectively, and the associated clinical consequences. A persistent, pro-inflammatory (M1-like) macrophage phenotype is typically associated with fibrosis and scarring. In contrast, an early transition to a regulatory, pro-remodeling (M2-like) macrophage phenotype is predictive of organized, site-appropriate connective tissue deposition. The ratio of M2-like to M1-like macrophages in the early post-implantation period defines the microenvironmental milieu and the associated tissue response. The present study evaluated the early macrophage response to a synthetic non-resorbable (Bard® Mesh), synthetic resorbable (TIGR® Matrix Surgical Mesh and GORE® BIO-A® Tissue Reinforcement), synthetic mesh composed of the naturally occurring molecule 4-hydroxybutyrate, (Phasix™ Mesh), and a biologic surgical mesh composed of dermal extracellular matrix (Strattice™ Reconstructive Tissue Matrix); all of which are used in ventral hernia repair. The spatiotemporal distribution of pro-inflammatory ($CD68^+CD86^+TNF\text{-}\alpha^+$) and pro-remodeling ($CD68^+CD206^+$) macrophages, and the remodeling response in terms of vascularization, total number of infiltrating cells, presence of multinucleate giant cells (MNGC), and cell layer thickness around the implanted materials was evaluated at 3, 7, 14, 21, and 35 days post implantation. Results showed an association of the synthetic non-resorbable and resorbable meshes with a robust, pro-inflammatory response within 3 days of implantation, and an increased presence of MNGC around the mesh fibers at longer time points. Phasix™ Mesh was associated with an increased presence of M2-like macrophages immediately adjacent to the mesh fibers at earlier time points, and a favorable tissue remodeling outcome at 35 days. Results of the present study are consistent with the premise that an early shift of M1-like to M2-like macrophages is associated with favorable outcomes, including reduced fibrosis, at later time points.

1. Introduction

Ventral hernia repair is one of the most common surgical procedures performed worldwide. More than one million ventral hernia repair procedures are performed each year in the US alone.[1] The use of a surgical mesh for this surgery has become commonplace, largely in response to the documented decrease in the incidence of hernia recurrence compared to repair without the use of a surgical mesh.[2,3] However, all meshes elicit a host tissue response that is dependent, in part, upon the material(s) from which the mesh is manufactured, the design and degradability of the material, and host variables such as age, body mass index, smoking history, and co-morbidities, among others.[4–9]

At the cellular level, innate and adaptive immune cells including neutrophils, macrophages, dendritic cells, and T cells, among others, play important roles in the host response to surgically implanted

* Corresponding author. Department of Surgery, Department of Bioengineering, McGowan Institute for Regenerative Medicine, University of Pittsburgh, 450 Technology Drive, Suite 300, Pittsburgh, PA, 15219, USA.
E-mail address: badylaks@upmc.edu (S.F. Badylak).

https://doi.org/10.1016/j.regen.2018.12.002
Received 30 May 2018; Received in revised form 7 December 2018; Accepted 20 December 2018
Available online 26 December 2018
2468-4988/ © 2019 Elsevier Inc. All rights reserved.

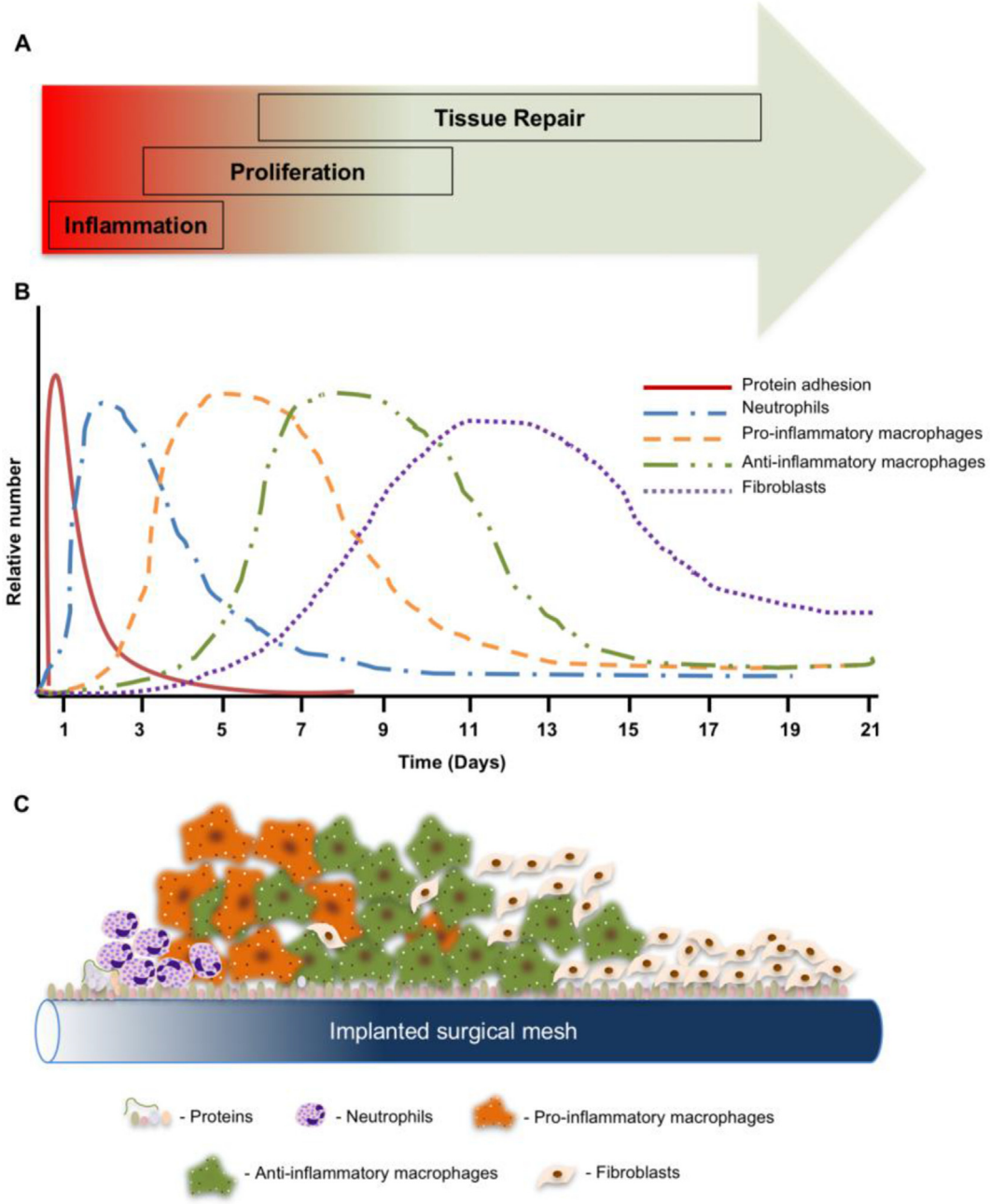

Fig. 1. Host response to biomaterials. A. Phases of healing process following an implantation of a surgical mesh material. **B.** Timeline of molecular and cellular events at the mesh-tissue interface. **C.** Schematic view of protein adhesion (Vroman effect), and cellular interactions with an implanted surgical mesh (A & B, adapted from [11,12]).

materials.[10] One of the major determinants of the downstream outcome following biomaterial implantation is the phenotype of the innate immune response, especially the macrophage component of the innate response (Fig. 1, adapted from [11,12]). Macrophage activation toward a pro-inflammatory (M1-like) or a pro-remodeling (M2-like) phenotype can occur by both independent and/or T-helper (Th) cell driven mechanisms.[13] Specifically, T-helper 1 (Th-1) activation induces a pro-inflammatory (M1-like) activation of macrophages, whereas T-helper 2 (Th-2) activation has been associated with tissue homeostasis and constructive remodeling mediated by M2-like macrophages.[14,15] In the context of surgically implanted mesh materials, persistent pro-inflammatory (M1-like) macrophage phenotype is typically associated with dense fibrosis and scar tissue formation and, if the implanted material is non-degradable, the well described foreign body response (FBR).[16–18] In contrast, a regulatory, pro-remodeling (M2-like) macrophage phenotype within the first 14 days post-implantation is predictive of the deposition of less dense, organized and site appropriate connective tissue.[19]

The initiators of a pro-inflammatory vs. a pro-remodeling macrophage response are not fully understood with respect to biomaterials; however, synthetic and non-degradable biomaterials typically induce a pro-inflammatory response, while naturally occurring, degradable materials typically induce a pro-remodeling response.[17,20,21] Neither of these phenotypes is exclusive and in reality, the ratio of cells with their respective phenotype defines and determines the microenvironmental milieu and associated tissue response.[17,19,22]

The objective of the present study is to characterize the host response induced by a subset of surgical meshes composed of synthetic

A

Commercial Scaffold Name	Polymer Composition	Category	*in vivo* Resorption Time	Fiber Diameter	Pore Size	Ref.
Phasix™	Poly-4-Hydroxybutyrate (P4HB)	Bioresorbable Monofilament	12-18 months	166 μm	0.25 mm^2	[26]
Bard®	Polypropylene (PP)	Non-resorbable Synthetic	NA	185.7 μm	0.44 mm^2	[27]
TIGR®	Fast Resorbing Fiber - Copolymer of Glycolide, Lactide and Trimethylene Carbonate (TMC) Slow Resorbing Fiber - Lactide and Trimethylene Carbonate	Synthetic Resorbable Multifilament	4 months & 36 months	10-40 μm	1.0 mm^2	[27, 28]
GORE® BIO-A®	Polyglycolic acid (PGA) & Trimethylene Carbonate (TMC)	Synthetic Resorbable Multifiber	6 months	3.38 μm	NA	[29]
Strattice™	Acellular Porcine Dermis	Biologic Graft	12 months	NA	NA	[30]

B

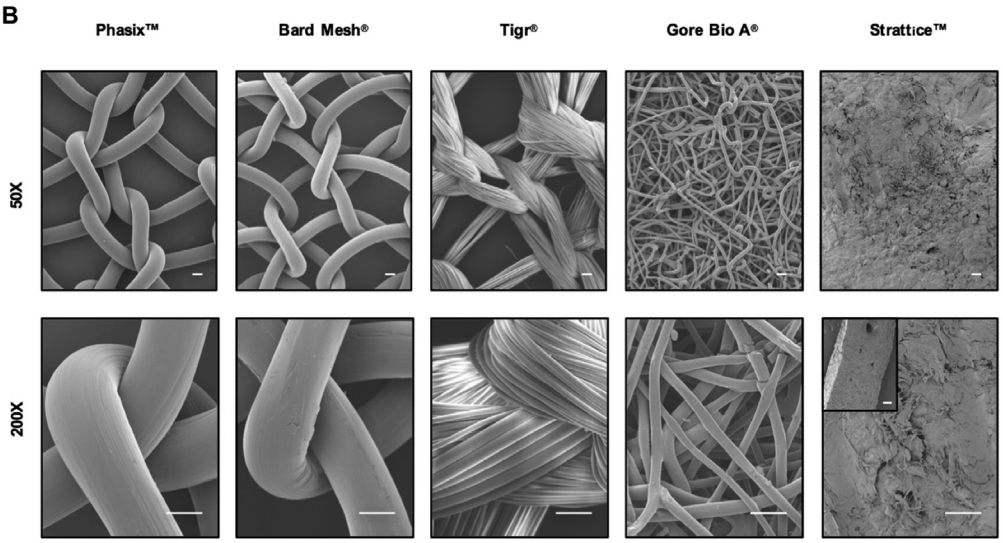

Fig. 2. Characteristics of surgical mesh devices. A. Composition and properties.[26–30] NA = not applicable because polypropylene is non degradable *in vivo*. **B.** Scanning electron microscopy of surgical mesh materials. SEM images of each mesh device at 50× magnification (upper row, scale bar 100 μm) and 200× magnification (bottom row, scale bar 100 μm). Inset represents the cross-sections of the biologic scaffold 50× magnification (scale bar 200 μm).

and naturally occurring biologic biomaterials, some of which were degradable and others non-degradable.

2. Materials and methods

2.1. Experimental design overview

The effects of selected surgical meshes upon macrophage activation were evaluated *in vivo*. Three synthetic surgical mesh devices: 1) Bard® Mesh (C.R. BARD, Warwick, RI, USA), 2) TIGR® Matrix Surgical Mesh (Novus Scientific, Sweden), 3) GORE® BIO-A® Tissue Reinforcement (W. L. Gore & Associates, Flagstaff, AZ, USA); 4) one mesh device composed of the naturally-occurring molecule 4-hydroxybutyrate, Phasix™ Mesh (C.R. BARD, Warwick, RI, USA)[23–25]; and 5) one biologic mesh device Strattice™ Reconstructive Tissue Matrix (LifeCell, Bridgewater, NJ, USA), were used in the present study (Fig. 2).[26–30]

In vivo study: A rat abdominal bilateral partial thickness defect was used to evaluate the host response to the implanted surgical mesh devices in comparison to unrepaired abdominal wall partial thickness defects (i.e., no implanted material).[19,31] The histologic appearance and macrophage phenotype were evaluated at 3, 7, 14, 21, and 35 days after surgery (Fig. S1).

In vitro study: Degradation products of the meshes generated by hydrolysis were used to either activate naïve murine bone marrow-derived macrophages for 24 h, or to challenge pre-activated $M_{IFN\text{-}\gamma/LPS}$ macrophages. Macrophage phenotype was evaluated by gene expression and immunolabeling for markers of macrophage activation (Fig. S1).

2.2. Scanning electron microscopy

Surface characteristics of the surgical meshes were evaluated by scanning electron microscopy (SEM). Strattice™ scaffold was fixed in aqueous glutaraldehyde solution (2.5% v/v) for 30 min, followed by immersion in a series of progressively greater concentrations of ethanol (30%, 50%, 70%, 90%, and 100%). The scaffold material was then dried in 100% hexamethyldisilazane (HMDS) (Sigma-Aldrich, MW, USA) for 3 min. All other evaluated surgical mesh materials did not require fixation or dehydration steps. The surgical mesh materials were mounted onto aluminum stubs and sputter coated with gold/palladium alloy (thickness: 4.0 nm). The meshes were imaged with a scanning electron microscope (JEOL JSM6330f, JEOL, Peabody, MA) at a 3.0 kV accelerating voltage.

2.3. Surgical model and mesh implantation

The host *in vivo* response to the implanted surgical meshes was evaluated using a previously described rat abdominal wall partial thickness defect model.[31,32] Animal procedures were approved by and performed according to the guidelines of the Institutional Animal Care and Use Committee at the University of Pittsburgh (IACUC protocol #15127009). Sixty Sprague–Dawley rats were randomly divided into six separate groups. Each rat was anesthetized and maintained at a surgical plane of anesthesia with 2% isoflurane in oxygen. The surgical site was prepared in sterile fashion using a betadine (providone-iodine) solution followed by placement of sterile drapes. Bilateral paramedian skin incisions were made to provide access to the muscular abdominal wall. Defects measuring 1 cm × 1 cm were created in the exposed musculature (external and internal oblique muscles), leaving the underlying peritoneum and transversalus fascia intact. The defects were then either repaired with one of the test articles or left unrepaired (n = 4 for each group at each time point). Each mesh was sutured to the adjacent abdominal wall musculature with 4–0 Prolene non-absorbable suture at each corner to secure the mesh and allow for partial mechanical loading of the test article, and to allow for identification of the implant boundaries at the time of euthanasia and explanation. A minimal amount of suture material was used to avoid eliciting a host response to the suture material that would obscure the host response to the mesh material itself. The skin was closed using absorbable 4–0 Vicryl suture. The animals were recovered from anesthesia on a heating pad and allowed normal activity and diet for the remainder of the study period.

2.4. Test article collection

At 3, 7, 14, 21, and 35 days post implantation, 2 animals in each group were euthanized by CO_2 inhalation and subsequent cervical dislocation in accordance with the guidelines of the American Veterinary Medical Association (AVMA) Panel of Euthanasia. Following euthanasia and using sterile technique, the skin was gently dissected and reflected, and the test specimens and surrounding tissue were collected and immersed in 10% Neutral Buffered Formalin (NBF) for subsequent histologic evaluation.

2.5. Quantitative histomorphologic analysis

A quantitative scoring system (Table S1) was used to evaluate the host response to the implanted surgical meshes at each time point. The NBF-preserved specimens were embedded in paraffin prior to being cut into 5 μm thick sections and mounted onto glass slides. The specimens were deparaffinized with xylene immersion followed by exposure to a graded series of ethanol solutions (100%, 95%, 75%).[17] Sections were stained with hematoxylin and eosin (H&E) (Sigma-Aldrich, USA) following manufacturer instructions. Stained slides were dehydrated using a graded series of ethanol solutions (75%, 95%, 100%) prior to coverslipping. A total of 3 low magnification (100×) and 3 high magnification (400×) images were acquired for each H&E section at the mesh-tissue interface. The criteria used to quantitatively evaluate the histomorphology of the specimens included: total cellular infiltration, vascularization, number of multinucleate foreign body giant cells (MNGC), and cell layer thickness around the implanted surgical mesh. The total number of cells per field of view (FOV) was quantified using CellProfiler Image Analysis Software (http://www.cellprofiler.org). All other scoring criteria were quantified by three independent blinded observers.

2.6. Immunolabeling of tissue sections

The macrophages within each FOV were identified and quantified by immunofluorescence. Antigen retrieval of tissue sections was facilitated with citrate buffer (10 mM citrate, pH 6.0) at 95–100 °C for 20 min. The blocking solution, consisting of 2%v/v normal horse serum (Hyclone), 1%wt/v bovine serum albumin (Sigma), 0.1%v/v Triton X-100 (Sigma), and 0.1%v/v Tween-20 (Sigma) in PBS, was applied for 1 h. Primary antibodies against the pan-macrophage marker CD68 (mouse anti-rat CD68, clone ED1, Abd Serotec) and the M1-like, pro-inflammatory macrophage marker CD86 (rabbit anti-human CD86, clone EP1158Y, Abcam) were used at 1:150 dilution, the M2-like, pro-remodeling macrophage marker CD206 (goat anti-human CD206, polyclonal, Santa Cruz) was used at 1:100 dilution, incubating overnight at 4 °C. Sections were washed and incubated with the following fluorescently conjugated secondary antibodies diluted in blocking solution for 1 h at room temperature: donkey anti-mouse Alexa Fluor-594 (1:200 dilution, Invitrogen), donkey anti-rabbit PerCPCy5.5 (1:300 dilution, Santa Cruz), and donkey anti-goat Alexa Fluor-488 (1:200 dilution, Invitrogen). Nuclei were labeled with DAPI and slides coverslipped with fluorescent mounting medium (Dako). Three multispectral epifluorescent images were acquired for each slide at the mesh-tissue interface (Nuance multispectral imaging system, CRi Inc.).

Macrophages were defined as CD68 positive co-localized with nuclei. The total number of cells co-expressing CD68 with CD86 and/or CD206 was quantified for each image using CellProfiler Image Analysis Software (http://www.cellprofiler.org). The subpopulation of macrophages $CD68^+CD206^+CD86^+$ was denoted as “triple-labeled”. The M1-like subpopulation was calculated by subtracting the number of triple-labeled $CD68^+CD206^+CD86^+$ cells from the $CD68^+CD86^+$ cells, to remove double counted cells. Likewise, the M2-like subpopulation of macrophages was calculated by subtracting the number of triple-labeled $CD68^+CD206^+CD86^+$ cells from the $CD68^+CD206^+$ cells. A ratio of the number of M2-like to M1-like cells ($(CD68^+CD206^+):(CD68^+CD86^+)$) was calculated for each field. The ratio was obtained dividing the number of M2-like macrophages by the number of M1-like macrophages.

Expression of TNF-α was evaluated following the protocol described above. The primary antibody (rabbit anti-human, Abcam Cat No. ab6671) and the goat anti-rabbit Alexa Fluor-488 (1:200 dilution, Invitrogen) were used. The percentage of cells co-expressing CD68 with TNF-α was calculated from the total number of cells for each image using CellProfiler Image Analysis Software (http://www.cellprofiler.org).

2.7. In vitro effect of degradation products of meshes upon macrophage phenotype

2.7.1. In vitro accelerated hydrolysis of degradable meshes

Phasix™ mesh was hydrolyzed with 3M HCl at 37 °C using a modification of a previously established accelerated hydrolysis method.[26] Tigr® Mesh and GORE® BIO-A® were hydrolyzed with 9M NaOH at 37 °C. Bard® Mesh was used as a non-degradable control. Solubilized monomers released by the hydrolysis were neutralized to pH 7.0 with the opposite solution. The resulting solution was dialyzed with a membrane

(0.1–0.5 Kd cut off) (Float-A-Lyzer™ G2 Dialysis Device, Fisher Scientific Cat No. 08-607-016) to remove the excess salt.

2.7.2. In vitro degradation of the ECM-based biologic scaffold

Degradation products of Strattice™ were obtained through enzymatic digestion.[33,34] 100 mg of pepsin (Sigma, Cat No. P7012) were mixed with 1000 mg of lyophilized Strattice™ powder in 100 ml of 0.01 M HCl. The digestion was performed for 48 h at a constant stir.

2.7.3. Isolation and culture of murine bone marrow-derived macrophages (BMDM)

All procedures were approved by and performed according to the guidelines of the Institutional Animal Care and Use Committee at the University of Pittsburgh (IACUC protocol #15086460). Bone marrow-derived monocytes were obtained from female C57bl/6 mice (Jackson Laboratories, Bar Harbor, ME) and differentiated into macrophages as previously described.[33] Animals were euthanized by CO_2 inhalation and subsequent cervical dislocation in accordance with the guidelines of the American Veterinary Medical Association (AVMA) Panel of Euthanasia. Following euthanasia and using an aseptic technique, the skin of the hind legs was completely removed, the coxa-femoral joint was disarticulated, and the legs harvested. The excess of muscle was removed, and after disarticulation of tarsus and stifle, tibia and femoral bones were isolated. Under sterile conditions, the ends of each bone were transected and the bone marrow flushed with medium using a 30G needle. Harvested monocytes were seeded at a concentration of 2×10^6 cells/ml and differentiated into macrophages by culture for 7 days with macrophage-colony-stimulating-factor (MCSF)-containing media [DMEM high glucose (Gibco, Grand Island, NY), supplemented with 10% fetal bovine serum (FBS) (Invitrogen, Carlsbad, CA), 10% L929 cell supernatant, 50 μM beta-mercaptoethanol (Gibco), 100 U/ml penicillin, 100 μg/ml streptomycin, 10 mM non-essential amino acids (Gibco), and 10 mM hepes buffer]. Cells were differentiated into macrophages for 7 days at 37 °C and 5% CO_2 with media changes every 48 h.

2.7.4. Cell viability assay

Viability of stimulated macrophages was measured using the MTT assay (Vibrant® MTT Cell Proliferation Assay Kit, V-13154, Molecular Probes) following the manufacturer instructions. Briefly, 1×10^5 bone marrow-derived monocytes were plated and differentiated into macrophages as described above. The degradation products of each surgical mesh were evaluated at 0.0207 mg/ml, 0.0415 mg/ml, 0.083 mg/ml, 0.165 mg/ml, 0.33 mg/ml, 0.66 mg/ml, 1.32 mg/ml, 2.64 mg/ml, 5.28 mg/ml, and 10.56 mg/ml for 24 h at 37 °C, 5% CO_2. After stimulation, macrophages were washed with phosphate buffered saline (PBS) and incubated with 100 μl of serum-free and antibiotic-free media containing 1.2 mM MTT (3-(4,5-dimethythiazol-2-yl)-2,5-diphenyltetrazolium bromide) solution for 2 h. After the incubation period, 75 μl of media was removed from each well and the formazan produced by reduction of the MTT was diluted with 50 μl of dimethyl sulfoxide (DMSO). Following an incubation period of 10 min at 37 °C, the concentration of formazan was determined by optical density at 540 nm. The metabolic activity of macrophages was calculated from a standard curve. Results were presented relative to untreated (media only) macrophages.

2.7.5. Macrophage activation

Naïve macrophages were stimulated with 1.32 mg/ml of the by-products of hydrolysis of synthetic meshes, 200 μg/ml of pepsin-digested Strattice™, or the macrophage activation controls to promote an M1-like phenotype (20 ng/ml IFNγ and 100 ng/ml of LPS) or an M2-like phenotype (20 ng/ml IL-4) for 24 h at 37 °C, 5% CO_2.[35,36] In a separate experiment, macrophages were first activated toward the pro-inflammatory phenotype using IFNγ and LPS for 6 h, as described above, followed by stimulation using the degradation products of the mesh materials for 24 h.[37]

2.7.6. Immunolabeling of in vitro treated macrophages

Stimulated macrophages were fixed in 2% paraformaldehyde for 30 min, followed by washes with PBS. Fixed cells were then incubated for 1 h with blocking buffer (2%v/v goat serum, 1%wt/v bovine serum albumin, 0.1%v/v triton X-100, and 0.1%v/v tween-20 in PBS) to inhibit non-specific binding of antibodies. After blocking, macrophages were incubated in primary antibodies at 4 °C overnight: (1) monoclonal rat anti-murine F4/80 (CI-A3-1) (Novus Biologicals, Cat. No. NB600-404) at 1:100 dilution, (2) polyclonal rabbit anti-iNOS (Novus Biologicals, Cat. No. NB300-605) at 1:100 dilution, (3) polyclonal rabbit anti-murine Fizz1 (RELMα) (Peprotech, Cat. No. 500-P214) at 1:100 dilution, and (4) polyclonal rabbit anti-liver Arginase (Abcam, Cat. No ab91279) at 1:100 dilution. After washing in PBS, the macrophages were incubated in fluorophore-conjugated secondary antibodies [Alexa Fluor goat anti-rat 488 (A11006) or goat anti-rabbit 488 (Cat. No. A11034), Invitrogen] at 1:200 dilution for 1 h at room temperature. After washing again with PBS, nuclei were counterstained with 4′-6-diamidino-2-phenylindole (DAPI) prior to imaging. Images of three 20× fields were taken for each well using a Zeus live-cell microscope, standardizing the light exposure times for based upon those set for cytokine-treated macrophages. The percent of positive cells for each marker was quantified using CellProfiler Image Analysis Software (http://www.cellprofiler.org), positive macrophages (green label) were identified by their co-localization with DAPI positive nuclei. The percent of expressing macrophages was then determined by dividing the identified positive cells by the total number of macrophage nuclei.

2.7.7. Gene expression profile of macrophages

Transcriptional activation of surface markers, metabolic markers, and transcription factors[37] was evaluated in macrophages exposed to the degradation products of each of the surgical meshes. Total RNA was extracted from stimulated macrophages with 800 μl TRIzol reagent (Ambion, Cat. No. 15596018) using cell scraper. The solution was mixed with 200 μl chloroform, vortexed for 15 s and centrifuged at 12,000 g for 10 min. The aqueous phase was transferred to a new tube and the RNA precipitated with 3M sodium acetate (1/10 of the volume) and isopropanol (1 vol), followed by centrifugation at 18,000 g for 20 min. RNA purification was made washing the RNA pellet in 75% ethanol with an additional centrifugation at 18,000 g for 15 min. The RNA pellet was air dried and re-suspended in nuclease-free water. The RNA solution was treated with DNase I to remove any residual genomic DNA. 1 μg RNA was converted in cDNA using the High Capacity cDNA Reverse Transcription Kit (Invitrogen, Cat. No. 4368814) following manufacturer instructions. Real time quantitative polymerase chain reaction (qPCR) was made using PowerUp™ SYBR® Green Master Mix (Applied Biosystems, Cat. No. A25778) to determine the levels of expression of different markers of macrophage activation. The levels of expression were normalized with the housekeeping gene hprt1. Results were expressed as fold change log ($2^{-\Delta\Delta Ct}$) relative to non-treated macrophages.

2.8. Statistical analysis

Quantification of histomorphologic criteria and immunolabeling are presented as the mean ± the standard error of the mean (SEM) from four biologic replicates. Data normality was evaluated using the Kolmogorov-Smirnov test for each mesh device at each time point. Statistical differences between the mesh materials at each time point were determined using a non-parametric ANOVA test (Kruskal-Wallis test). The pattern of differences was evaluated with post-hoc Dunn's multiple comparison test. A value $p < 0.05$ was considered statistically significant. Statistical analysis was performed using GraphPad Prism version 7.0c (GraphPad Software, La Jolla CA, USA).

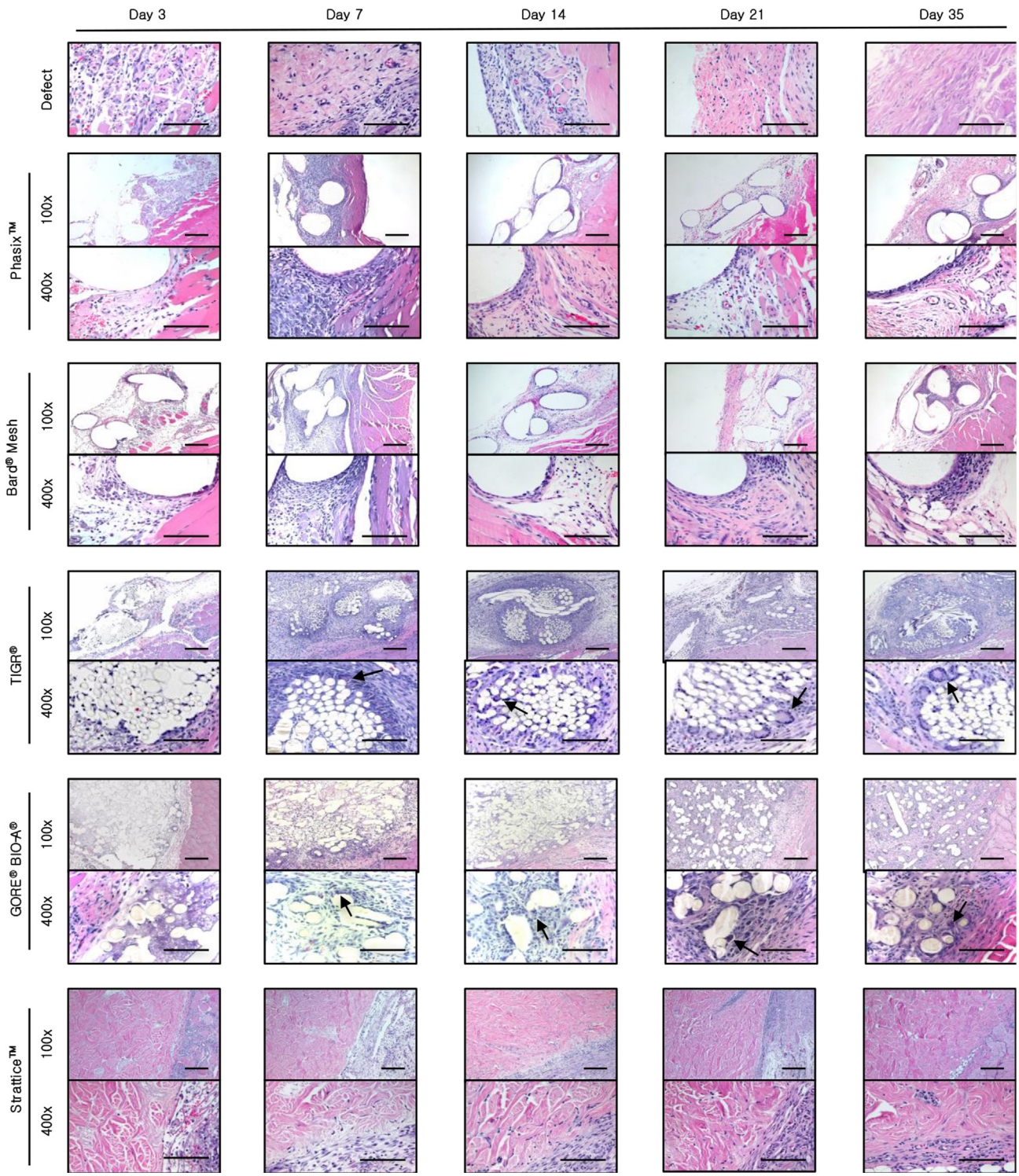

Fig. 3. Histologic appearance of the host response to implanted surgical meshes. Representative hematoxylin and eosin stained histologic cross sections of unrepaired abdominal wall partial thickness defects or each mesh at 3, 7, 14, 21, and 35 days post-implantation. The surgically created defect involved focal removal of the internal and external abdominal oblique muscles while leaving the transversalis muscle layer intact. The images show the cell response to the defect alone or the defect repaired with surgical meshes: Phasix™ Mesh, Bard® Mesh, TIGR®, GORE® BIO-A®, and Strattice™. Low magnification images (100×, upper, scale bar 200 μm) show the extent of vascularization and cellular infiltration. High magnification images (400×, bottom, scale bar 100 μm) show the MNGC and the cell layer thickness at the margins of the implanted materials. Black arrows identify the presence of MNGC in each FOV.

3. Results

3.1. Macroscopic assessment

All animals survived to the intended time point. All implanted surgical meshes were integrated with surrounding tissue. By day 35, all implanted materials remained largely intact and were easily identified during necropsy. None of the implanted test articles induced edema at the implant site.

3.2. Histomorphologic quantification

The host tissue remodeling response was quantified from H&E stained images (Fig. 3) with respect to vascularization, total number of infiltrating cells, presence of MNGC, and thickness of the cells layers around the implanted material. At each time point, non-parametric test indicated that the level of vascularization per FOV around the implanted surgical meshes remained comparable (Fig. S2A). After 35 days of implantation, the number of vessels found at the mesh-tissue interface ranged between 6 and 12 per 100× FOV.

The acute host response (days 3 and 7) to all materials was characterized by a dense infiltration of mononuclear cells. TIGR® mesh showed greater infiltration of mononuclear cells compared with the other meshes at all time points (Fig. S2B). The presence of MNGC was noted in H&E stained images at 400× FOV (Fig. 3). Differences in the number of MNGC between the surgical meshes were evident as early as day 7 post-implantation, as shown in Fig. S2C. By day 7, quantification of these cells showed (2.50 ± 0.25) MNGC around Phasix™, (2.27 ± 0.13) MNGC around Bard® Mesh, (3.94 ± 0.11) cells around GORE® BIO-A®, (11.78 ± 0.47) cells around TIGR®, and (0.44 ± 0.22) cells around Strattice™. These values remained consistent by day 35 for each of the meshes, as shown in Fig. S2C. Further analysis indicated that there were significant differences ($p < 0.05$) in the number of MNGC between Strattice™ and TIGR® mesh at 7, 14, 21, and 35 days (Fig. S2C and statistical analysis Table S2).

The number of cell layers in the area of dense accumulation immediately adjacent to each of the TIGR®, GORE® BIO-A®, and Strattice™ devices remained constant at all time points. Phasix™ mesh showed an increased cell layer thickness around the fibers at day 7. At this time point, cell layer thickness around Phasix™ was statistically different compared with GORE® BIO-A® ($p < 0.05$) but not compared to any of the other meshes (Table S2). The cell layer thickness around Phasix™ decreased over time. For all the other time points (days 14–35), the cell layer thickness around the implanted material remained similar between the meshes (Fig. S2D and Table S2).

3.3. Spatiotemporal analysis of macrophage phenotype

The spatiotemporal distribution of phenotypically distinct macrophages at the material-tissue interface was characterized by immunolabeling. The co-expression of the pan-macrophage cell surface marker CD68 with the pro-inflammatory (M1-like) CD86 marker and/or the pro-remodeling (M2-like) scavenger receptor CD206 was determined (Fig. 4). As shown in the defect control (i.e., no implanted material), earlier time points (days 3 and 7) were associated with a pro-inflammatory response at the wound site, with marked infiltration of $CD86^+$ macrophages. The response transitioned into a pro-remodeling reaction by day 14, when an increased population of $CD206^+$ macrophages was observed. A resolution phase without prolonged macrophage response was found at day 35 in normal tissue. Analysis of the M2-like:M1-like ratio for the defect control showed the lowest ratio by day 3 (0.29 ± 0.07), and increased values by day 14 (0.74 ± 0.15), day 21 (0.87 ± 0.52), and day 35 (1.05 ± 0.30) (Fig. 5).

All implanted surgical meshes induced a macrophage response that, although variable in phenotype remained active for the 35 days of evaluation. Infiltrated macrophages were localized at the biomaterial-tissue interface and in close proximity to the mesh fibers of Phasix™, Bard® Mesh, TIGR® and GORE® BIO-A®, and at the periphery of the Strattice™ scaffold (Fig. 4).

Day 3: By 3 days, the population of pro-inflammatory (M1-like) macrophages, recognized as $CD68^+CD86^+$ cells, was similar among the implanted materials (Fig. S3A, Day 3). However, the pro-remodeling (M2-like) subpopulation of macrophages, identified as $CD68^+CD206^+$, showed variability among the materials. Macrophages with an M2-like phenotype were in greatest number around Phasix™ (46.50 ± 13.19 cells), with fewer cells around Bard® Mesh (31.83 ± 12.82 cells), GORE® BIO-A® (30.54 ± 7.76 cells), Strattice™ (10.75 ± 2.83 cells), and the least number of M2-like macrophages around TIGR® (7.25 ± 3.89 cells). Statistical analysis of the M2-like macrophage population at this time point showed differences between the materials. The differences were greatest ($p < 0.05$) between Phasix™ vs. TIGR® and GORE® BIO-A® vs. TIGR®, as indicated in Fig. S3B, Day 3, and Table S3. Likewise, quantification of triple-labeled $CD68^+CD206^+CD86^+$ macrophages showed the greatest number around GORE® BIO-A® (44.54 ± 6.45 cells), with fewer cells around Phasix™ (42.50 ± 10.94 cells), Bard® Mesh (30.17 ± 8.90 cells), Strattice™ (25.37 ± 8.18 cells), and the least number of triple-labeled cells around TIGR® (12.75 ± 2.38 cells). Statistical analysis showed differences for this subpopulation of macrophages between the implanted materials, as indicated in Fig. S3C, Day 3 and Table S3. Differences observed in the subpopulations of macrophages for each of the implanted materials was reflected in the ratio of M2-like:M1-like macrophages. Analysis of the M2-like:M1-like ratio at day 3 showed a differential response among the materials. The ratio was higher for Phasix™ (4.44 ± 3.33) than for TIGR® (0.13 ± 0.03) ($p < 0.05$) (Fig. 5A and Table S3). None of the other materials were significantly different.

Day 7: The macrophage response at 7 days was distinct among the evaluated meshes. A predominant pro-inflammatory response was seen at the interface of the implanted TIGR® material, whereas all the other materials were characterized by a mixed population of macrophages (Fig. 4, column 2). Macrophages with an M1-like phenotype were in the greatest number around TIGR® (404.3 ± 78.6 cells), with fewer M1-like cells around Bard® Mesh (152.5 ± 20.8 cells), Phasix™ (147.50 ± 55.79 cells), GORE® BIO-A® (143.25 ± 19.73 cells), and the least number of M1-like macrophages around Strattice™ (31.00 ± 7.08 cells) (Fig. S3A, Day 7). Statistical differences were found between Strattice™ compared to either TIGR, Bard® Mesh, and GORE® BIO-A® ($p < 0.05$) (Table S3). The number of pro-remodeling M2-like macrophages was lower ($p < 0.05$) around the implanted Strattice™ scaffold compared to the other materials (Fig. S3B, Day 7, and Table S3). At day 7, the number of cells co-expressing $CD68^+CD206^+CD86^+$ also showed differences between the materials. The number of this subtype of macrophages was higher ($p < 0.05$) around TIGR® (70.33 ± 9.60 cells) when compared to Strattice™ (13.75 ± 3.83 cells) and Phasix™ (15.66 ± 5.10 cells) (Fig. S3C, Day 7, and Table S3). Statistical analysis of the M2-like:M1-like ratio at day 7 showed differences between the implanted meshes. The M2-like:M1-like ratio was higher ($p < 0.05$) around Phasix™ (2.06 ± 1.09 cells) than around TIGR® (0.12 ± 0.02 cells) and Strattice™ (0.08 ± 0.02 cells), respectively (Fig. 5B and Table S3). None of the other ratios were statistically significant.

Day 14: By day 14, the macrophage response remained a mixture of M1-like and M2-like cells for all materials (Fig. 4, column 3). The number of macrophage subtypes varied among the implanted materials. Phasix™ showed a higher number ($p < 0.05$) of both pro-inflammatory M1-like (205.00 ± 29.14) and pro-remodeling M2-like (41.17 ± 10.34) macrophages compared with Strattice™ (66.08 ± 23.19 and 11.42 ± 3.57, respectively) (Figs. S3A and S3B, Day 14, and Table S3). Likewise, TIGR® showed an increased ($p < 0.05$) subpopulation of cells co-expressing $CD68^+CD206^+CD86^+$ (84.50 ± 13.85) when compared with Strattice™ (11.17 ± 3.83) and GORE® BIO-A® (26.58 ± 7.47), respectively (Fig. S3C, Day 14, and Table S3). At this time point, the ratio of M2-like:M1-like macrophages did not show differences between the surgical materials (Fig. 5C and Table S3).

Day 21: After 21 days, the macrophage response to the implanted surgical meshes persisted as a mixture of phenotypic subtypes. The number of pro-inflammatory and pro-remodeling macrophages were similar among the materials (Figs. S3A and S3B, and Table S3); and therefore no differences were observed between the M2-like:M1-like ratios (Fig. 5D). In contrast, TIGR® was associated with an increased number ($p < 0.05$) of macrophages co-expressing

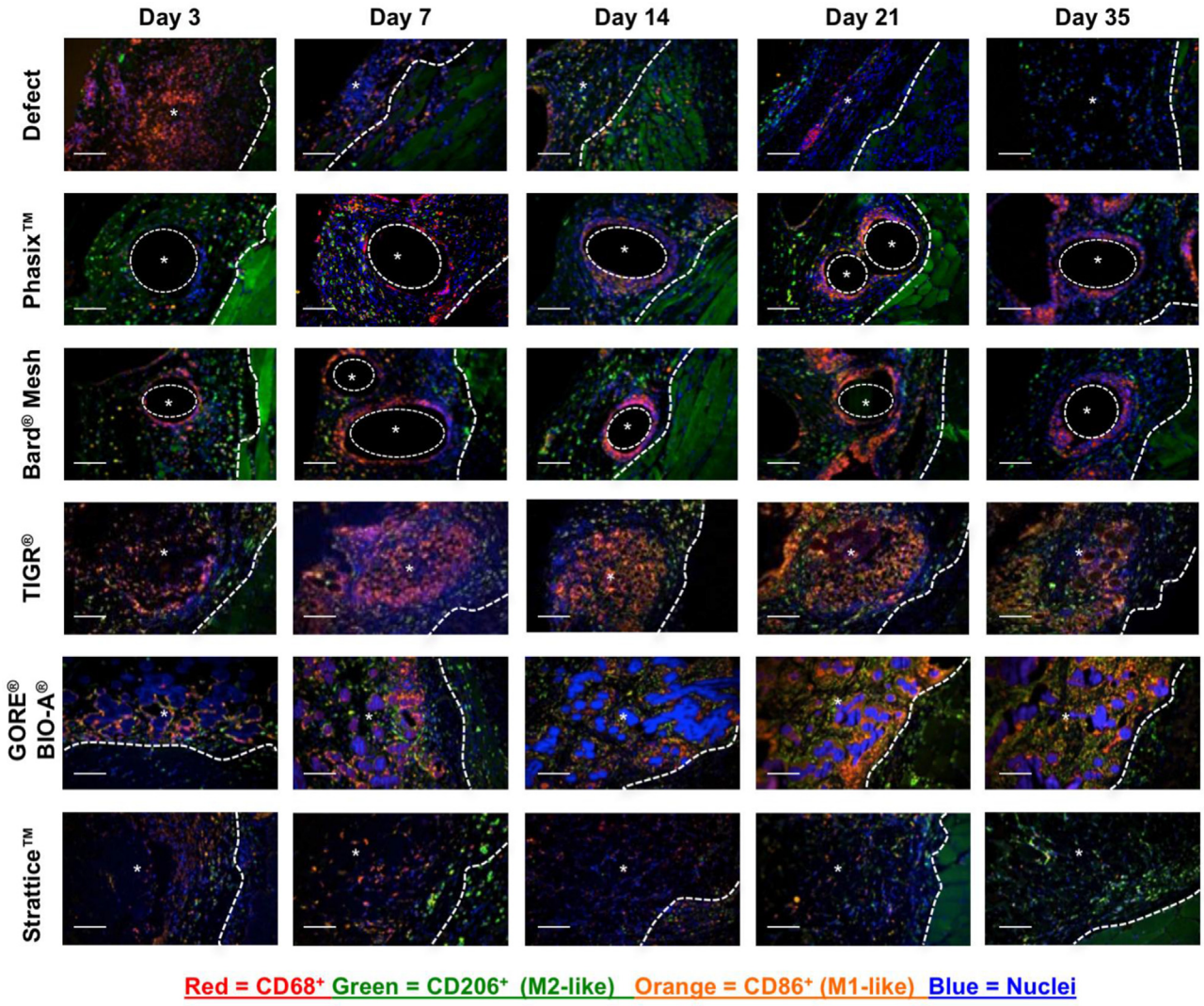

Fig. 4. Scaffolds composed of P4HB modulate an early anti-inflammatory phenotype of macrophages. Immunolabeling of implanted mesh materials or defect alone controls. Red: $CD68^+$ (pan macrophages), Green: $CD206^+$(pro-remodeling macrophages), Orange: $CD86^+$ (pro-inflammatory macrophages), Blue: DAPI. Earlier time points were characterized by a pro-inflammatory acute host response surrounding the implanted synthetic materials and the defect alone in contrast with a markedly pro-remodeling population of macrophages surrounding the Phasix™ mesh device. Scale bar 100 μm. (For interpretation of the references to colour in this figure legend, the reader is referred to the Web version of this article.)

$CD68^+CD206^+CD86^+$ (99.50 ± 16.70) compared with either Phasix™ (35.92 ± 8.27), GORE® BIO-A® (35.50 ± 6.58), and Bard® Mesh (47.08 ± 15.72) (Fig. S3C, Day 21, and Table S3).

Day 35: A mixed macrophage activation profile continued by day 35 at the interface of all implanted materials (Fig. 4, column 5). A significant change was observed for the number of M1-like macrophages associated to each of the implanted materials. The number of pro-inflammatory macrophages decreased at the periphery of Strattice™ (12.83 ± 2.70 cells) compared with either Phasix™ (163.66 ± 18.11 cells), Bard® Mesh (108.50 ± 13.52 cells), and TIGR® (86.83 ± 7.09 cells) ($p < 0.05$) (Fig. S3A, Day 35, and Table S3). At this time point, however, no differences were observed between the pro-remodeling M2-like macrophages (Fig. S3B, Day 35, and Table S3), and as a consequence, an increased ($p < 0.05$) M2-like:M1-like ratio was associated to Strattice™ (1.86 ± 0.57) compared with Phasix™ (0.18 ± 0.05) and Bard® Mesh (0.35 ± 0.12), respectively (Fig. 5E, and Table S3). The number of triple-labeled $CD68^+CD206^+CD86^+$ macrophages also showed differences between the meshes. TIGR® continued with increased values of this subpopulation of cells (83.67 ± 11.59 cells), as observed since day 7, and by day 35 were significantly higher ($p < 0.05$) compared with each of the other materials: Bard® Mesh (19.33 ± 3.51 cells), GORE® BIO-A® (19.50 ± 3.25 cells), Phasix™ (19.25 ± 3.34 cells), and Strattice™ (29.17 ± 6.08 cells) (Fig. S3C, Day 35, and Table S3).

Expression of macrophages ($CD68^+$) expressing the pro-inflammatory marker TNF-α was also evaluated at the mesh-tissue interface at all time points (Fig. S4). All meshes induced the expression of TNF-α at early time points (days 3 and 7). However, a persistent pro-inflammatory TNF-α expression, day 35, was observed around Bard® Mesh, TIGR®, and GORE® BIO-A® in comparison to the expression of this marker around Phasix™ and Strattice™.

3.4. In vitro macrophage response induced by degradation products of mesh scaffolds

The macrophage metabolic activity and the cytotoxicity induced by degradation byproducts of the surgical meshes were evaluated. Concentrations higher than 1.32 mg/ml of some of the degradation products were associated with a cytotoxic effect (Fig. 6A). Using the highest non-cytotoxic concentration of degradation products of the surgical meshes, the phenotypic profile of murine BMDM was determined by immunolabeling via the expression of the pan-macrophage

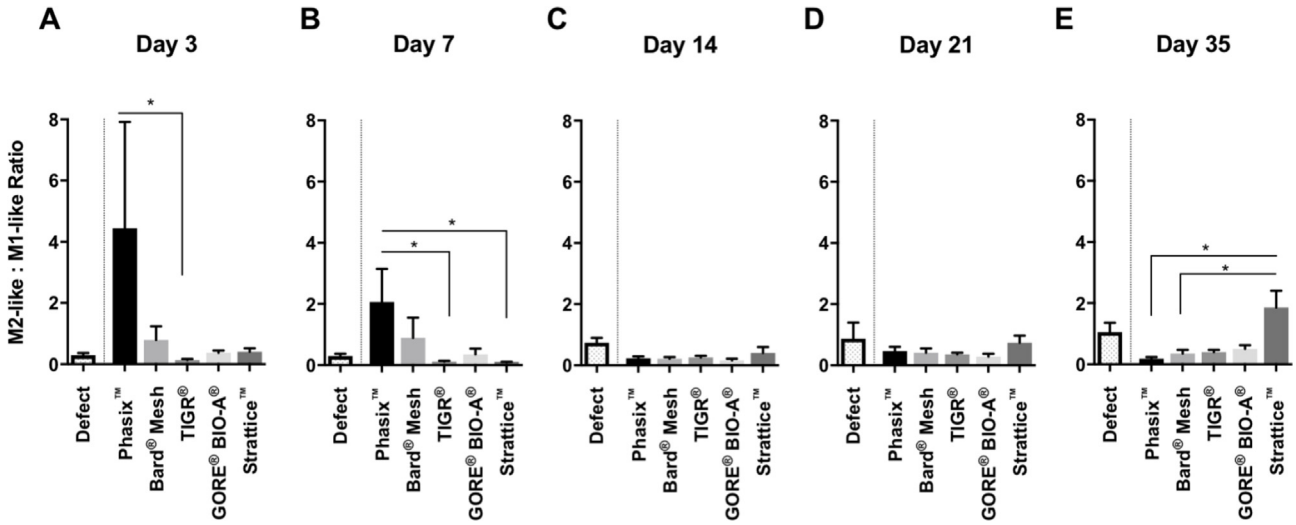

Fig. 5. Quantification of M2-like:M1-like ratio of macrophages. Ratio of M2-like:M1-like around mesh fibers at **A.** 3 days, **B.** 7 days, **C.** 14 days, **D.** 21 days, and **E.** 35 days. Images were quantified using Cell Profiler image analysis software. *In vivo,* Phasix™ mesh device modulates an earlier transition of pro-inflammatory to anti-inflammatory macrophages compared to synthetic mesh materials. Values: Mean ± SEM, N = 3, triplicate. Differences between stimuli for each marker were evaluated using non-parametric ANOVA test. Statistical significance was determined by $p < 0.05$.

marker F4/80, the pro-inflammatory marker iNOS, and the M2-like markers Fizz1 and Arginase1. Exposure of the macrophages to the degradation products of TIGR® and Strattice™ resulted in a statistically significant ($p < 0.05$) phenotypic response of iNOS. (Fig. 6B and C).

3.5. Immunomodulatory effect of degradation products of mesh materials upon pro-inflammatory macrophages

When BMDM were activated toward the pro-inflammatory phenotype by exposure to IFN-γ and LPS, followed by exposure to the degradation products of the meshes, significant changes in the phenotypic profile were observed (Fig. 7A). Exposure of macrophages to degradation products of TIGR® and GORE® BIO-A® showed an increase in the number of cells expressing iNOS ($p < 0.05$) (Fig. 7A). The degradation products of Phasix™ decreased ($p < 0.05$) the percentage of cells expressing F4/80, and increased ($p < 0.05$) the number of macrophages expressing Fizz1 and Arginase1, when compared with the other degradation products or the media control (Fig. 7B). At the mRNA level, degradation products of Phasix™ induced the transcriptional upregulation of the surface markers Fizz1 and IL1-Ra, and the transcription factors IRF3, KLF4, and STAT3 on macrophages first activated with LPS and IFN-γ (Fig. 7C).

4. Discussion

Macrophage response is a critical determinant of the host response.[38,39] Once thought to function primarily or exclusively as a phagocyte in response to infectious agents, foreign materials, and/or damaged tissue, and to occasionally combine with neighboring cells to form multinucleate giant cells as part of the foreign body reaction,[16,40] it is now recognized that macrophages have the potential for marked plasticity and have essential roles in diverse physiologic processes.[41,42]

Macrophages have antigen-presenting functions that link the innate and adaptive arms of the immune system,[43] participate in fetal and post-natal development,[44,45] tissue homeostasis,[46,47] and even tissue and organ regeneration.[48–51] Perhaps most surprising when considering present knowledge of macrophage biology compared to just 20 years ago, these cells show remarkable diversity with respect to their phenotype and secretome and play a crucial role in mitigating, not promoting, inflammation.[52] Of relevance to the present study, the macrophage phenotype induced within the first 14 days following implantation of a biomaterial has been associated with downstream tissue remodeling and functionality of the repaired tissue.[17,19]

The present study showed a distinctive temporal macrophage phenotype response to five different surgical meshes that differ in composition and degradability. The Bard® mesh is a non-degradable mesh composed of the synthetic material polypropylene and elicited a dominant M1-like response as expected.[17,18]

The two degradable synthetic surgical meshes, TIGR® and GORE® BIO-A®, also elicited an M1-like response with the TIGR® mesh showing a more robust pro-inflammatory response and accumulation of multinucleate giant cells than GORE® BIO-A®. Pre-clinical studies evaluating TIGR® or GORE® BIO-A® have shown that the pro-inflammatory response continues throughout the time that the materials are present at the implant site.[53–55] The cause for the more pronounced M1-like response to the TIGR® mesh is unknown but may be related to composition, knit pattern, degradation rate, and/or the degradation products, among other variables.[3,56,57] TIGR® mesh is composed of multifilament fibers that have different degradation rates depending upon the presence or absence of glycolide. The fast resorbing co-polymer is formed by glycolide, lactide, and trimethylene carbonate (TMC), and is hydrolyzed within the body in four months. The slow resorbing co-polymer, formed by lactide and TMC, takes three years to degrade.[54] In contrast, GORE® BIO-A® is a mesh composed of monofilament fibers of a co-polymer of glycolide and TMC, with an *in vivo* degradation time of 6 months.[55] TIGR® and GORE® BIO-A® have shown different rates of hernia recurrence, depending on whether they are used to treat lateral or medial inguinal hernias.[58] And more specifically, the rapid rate of degradation of GORE® BIO-A® has been associated with lower mechanical strength at the tissue repair site when compared with native muscle.[59]

Strattice™ is a slowly degradable biologic mesh composed of porcine dermal extracellular matrix (ECM). Most biologic meshes composed of ECM that are not chemically cross-linked are associated with a more favorable M2-like:M1-like ratio than synthetic meshes. However, tissue processing methods, including residual decellularization agents and preservatives can markedly influence the host response toward a pro-inflammatory state.[60,61] Strattice™ has previously been shown to cause a more dominant pro-inflammatory response than other biologic surgical meshes.[19,55]

Although the M2-like to M1-like ratio of macrophages around Strattice™ at 35 days was higher than the ratio found for the other surgical meshes, other studies have shown encapsulation of the implanted Strattice™ scaffold, increased expression of collagen I, and non-

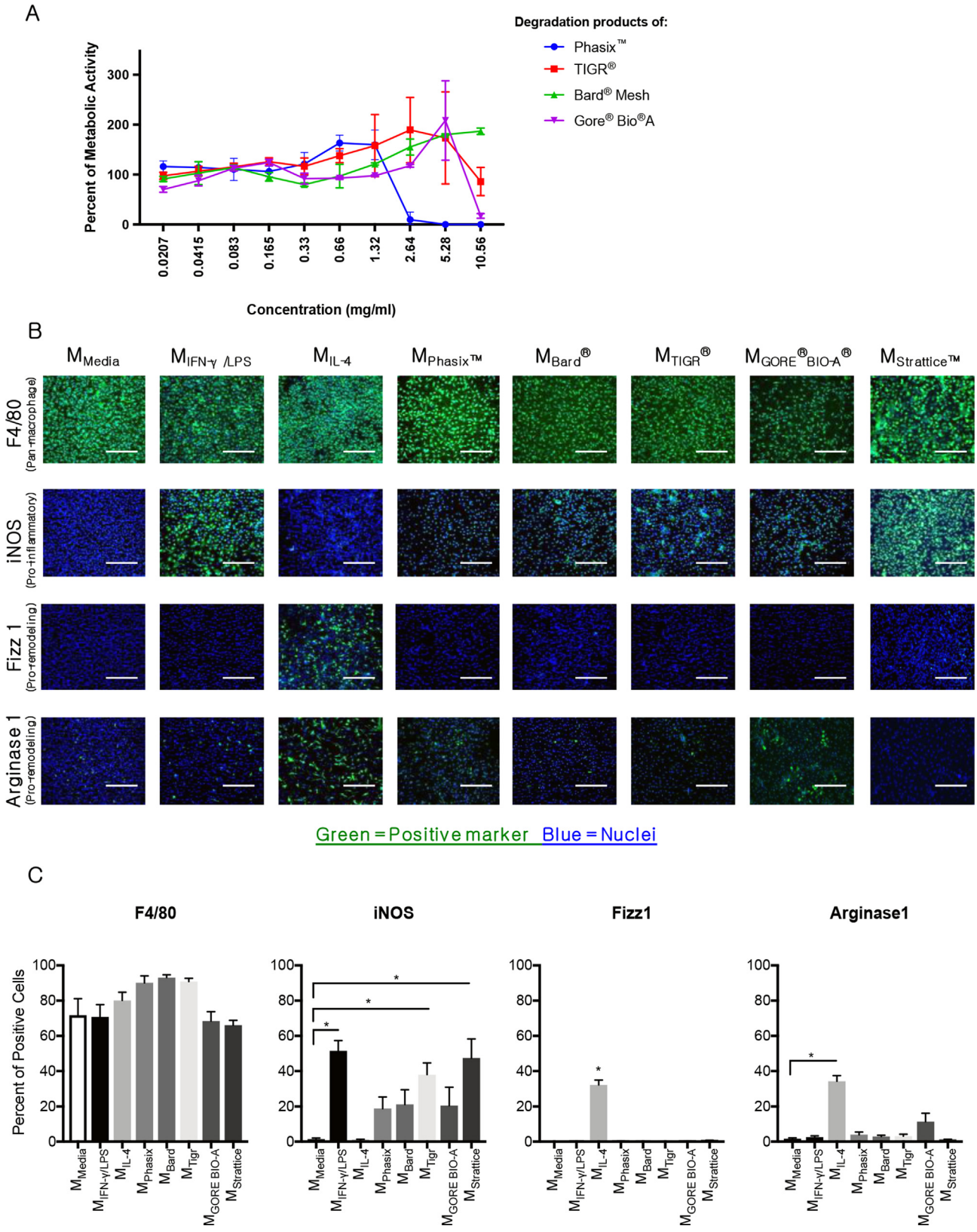

Fig. 6. *In vitro* macrophage response to degradation products of meshes. A. Dose response curves of degradation products of surgical meshes. **B.** Degradation products of TIGR® and Strattice™ promote an iNOS$^+$ macrophage phenotype. Primary murine BMDM were exposed to 1.32 mg/ml degradation products of Phasix™, TIGR®, GORE® BIO-A®, or Strattice™ for 24 h. Activation of markers associated with pro-inflammatory (iNOS) and anti-inflammatory (Fizz1 and Arginase1) phenotypes was evaluated by immunolabeling. A general marker of macrophages (F480), was used. Known factors that are promoters of pro-inflammatory (100 ng/ml LPS and 20 ng/ml IFN-γ) or anti-inflammatory (20 ng/ml IL-4) phenotypes were included as controls. Scale bar 200 μm. **C.** Quantification of the response of treated macrophages in A. Images were quantified using Cell Profiler image analysis software. Values: Mean ± SEM, N = 3, triplicate. Differences between stimuli for each marker were evaluated using non-parametric ANOVA test. Statistical significance was determined by $p < 0.05$.

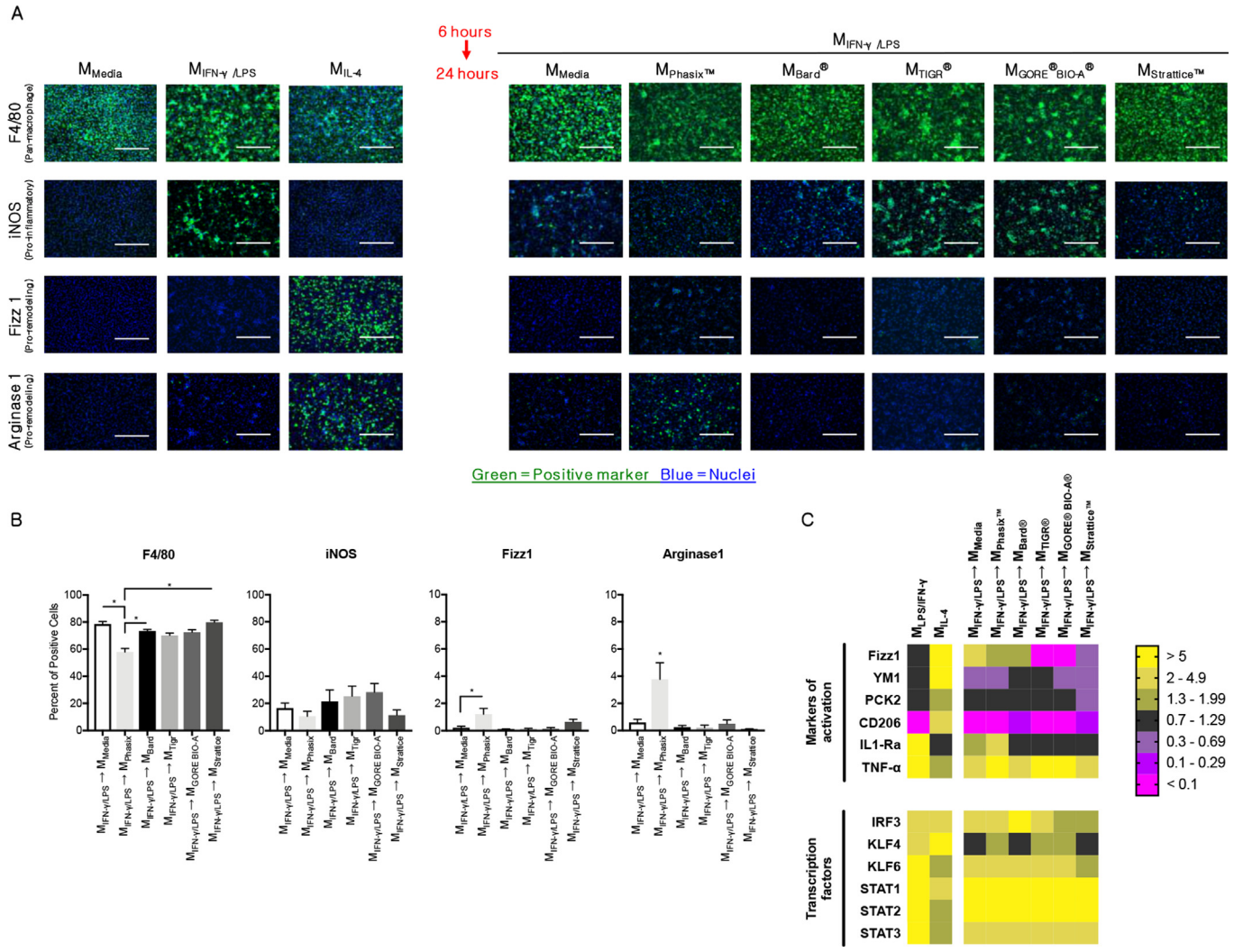

Fig. 7. Effect of degradation products of mesh materials upon pro-inflammatory macrophages. A. Degradation products of P4HB have an immunomodulatory effect upon pre-activated pro-inflammatory macrophages. BMDM were challenged with 100 ng/ml LPS and 20 ng/ml IFN-γ for 6 h to induce a pro-inflammatory phenotype, followed by exposure to 1.32 mg/ml degradation products of each of the mesh materials (Phasix™, TIGR®, GORE® BIO-A®, or Strattice™) or media alone for 24 h. Activation of markers associated with pro-inflammatory (iNOS) and anti-inflammatory (Fizz1 and Arginase1) phenotypes was evaluated by immunolabeling. The pan macrophage marker F480 was used. Known factors that are promoters of pro-inflammatory (100 ng/ml LPS and 20 ng/ml IFN-γ) or anti-inflammatory (20 ng/ml IL-4) phenotypes were included as controls. Scale bar 200 μm. **B.** Quantification of the response of challenged macrophages in A. Values: Mean ± SEM, biologic replicates (N) = 3, technical replicates = 3. Differences between stimuli for each marker were evaluated using non-parametric ANOVA test, *$p < 0.05$. **C.** Heat map of relative transcriptional activity of surface and metabolic markers, and transcription factors of macrophage changes after LPS/IFN-γ activation and followed by stimulation with degradation products. Data presented as fold change relative to non-treated macrophages.

degradation of the scaffold over a period of 180 days of study.[55] These results provide insight into the relationship of an early transition of macrophages from a pro-inflammatory to a pro-remodeling functional phenotype. Concerns have been raised regarding the high variability in the degradation rate of the Strattice™ scaffold, with speculation about differences in the anatomic location of the source tissue and reproducibility of clinical results.[62]

Phasix™ is a surgical mesh[23–25] composed of a naturally occurring (i.e., biologic origin) monomer 4-hydroxybutyrate that is manufactured as a polymer by synthetic methods. Hydroxylated and non-hydroxylated forms of butyrate are naturally occurring molecules that belong to the group of short chain fatty acids. Butyrate is produced in abundant amounts by bacteria in the gastrointestinal tract to protect against chronic inflammation,[63,64] whereas 4-hydroxybutyrate (4HB) is produced in various tissues as a neurotransmitter[65] and with protective effects against stress and ischemia.[66] Other hydroxylated isoforms of butyrate are modulators of metabolism during ketosis and insulin-resistance.[67,68] The ability to knit the polymeric form of 4-hydroxybutyrate provides the potential to create a surgical mesh with predictable mechanical properties. One of the hypothesized physiologic functions of 4HB, which is the hydrolytic degradation product of Phasix™, is the activation of an M2-like, or regulatory macrophage phenotype. Results of the present study show the increased presence of $CD206^+$ macrophages immediately adjacent to Phasix™ mesh fibers at early post-implantation time points. Previous studies have shown that the presence of pro-remodeling M2-like macrophages in the early post-implantation period biomaterials portends a favorable tissue remodeling outcome.[17,19,20] The present 35-day rat study shows an early M2-like macrophage response which is consistent with favorable long-term tissue remodeling outcomes observed in a 12-month pig study and 18-month clinical data.[25,69] Phasix™ has shown a lower incidence of hernia recurrence (9% after 18 months) when compared with other materials, such as Strattice™ (19% at 12 months and 28% at 24 months) or GORE® BIO-A® (17% at 24 months).[69]

It is clear from the results presented herein that the host response to different surgical mesh materials is distinctive. It has been suggested

that the host response to biomaterials is the single most important determinant of the remodeling and functionality of the repaired tissue.[70] Although other variables in surgical mesh properties such as strength, degradability and cost are important considerations, the host response will largely determine functionality, the incidence of complications and other clinical metrics of success vs. failure. The present study focused on the innate immune response, specifically the macrophage response. The host response however involves both innate and adaptive immune activation,[71] and a direct crosstalk occurs between the cells that mediate these immune responses. Further studies evaluating the role of T cells in response to the implanted surgical scaffolds is warranted.

The present study evaluated the *in vitro* expression of a group of surface markers, secreted molecules, and transcription factors commonly associated with LPS/IFN-γ-induced (iNOS, TNF-α, IRF3, STAT3) or IL-4-induced (Arginase 1, Fizz1, YM1, CD206, PCK2, IL1-Ra, KLF4, IL-10) responses by either providing a positive feedback and therefore accentuating a particular function or initiating a negative response that modifies the original phenotype. Results showed that macrophages activated with LPS and IFN-γ and then stimulated with 4HB induced a distinct pattern of expression characterized by the upregulation of important markers associated with the anti-inflammatory phenotype (Fizz1, Arginase 1, and IL1-Ra), as well as transcriptional upregulation of the transcription factor KLF4, all of which suggest a reparative immunomodulatory effect upon macrophages. Stimulated macrophages were also shown to upregulate the expression of TNF-α, and the transcription factors IRF3 and STAT3. It has been suggested that after stimuli of cells with SCFA, there is a tight regulation of both pro- and anti-inflammatory responses that allow the release of ROS, but also that modulate their activation state through the activation of a negative feedback mediated by G-protein coupled (GPR) receptors,[72] which in turn, might explain the pattern of macrophage phenotype being expressed after 4HB induction.

There are several limitations to the present study. Limited markers (CD86, CD206, TNF-α) were used to determine the phenotype of macrophages present at the mesh-tissue interface. These markers have been used to identify macrophages pushed to a pro-inflammatory ($CD86^+$) activation state or an anti-inflammatory and regulatory activation state ($CD206^+$) by non-physiologic amounts of cytokines, LPS + IFN-γ and IL-4, respectively.[41] Additional characterization of the phenotypic profile of the subpopulations of macrophages in both *in vivo* and *in vitro* studies, by using other surface, metabolic, and secreted markers would represent a more comprehensive characterization of phenotype. In addition, these meshes represent only a small subset of synthetic and biologic meshes. Therefore conclusions may not extend to other meshes within these three groups.

5. Conclusion

Results of the present study show that the temporospatial macrophage response to surgical meshes that differ in composition, rate of degradation, and structure are distinct and different. Further, it appears that 4HB, the degradation product of Phasix™, activates macrophages to a pro-remodeling M2-like phenotype in the early post-implantation time frame in contrast to a pro-inflammatory M1-like phenotype that is associated with the other tested surgical meshes. A more complete understanding of the factors influencing the patterns of macrophage activation, and the molecular interactions of mesh materials with cells could influence the design of meshes tailored to promote site appropriate tissue repair.

Conflicts of interest

Becton, Dickinson and Company/CR Bard sponsors research in the Badylak Laboratory at the University of Pittsburgh.

Acknowledgements

Catalina Pineda Molina was supported by the Colciencias-Fulbright Scholarship and the Tuition Remission Fellowship (TRF) from The Center for Latin American Studies (CLAS) at the University of Pittsburgh. The authors thank Lori Walton from the Histology Center at the McGowan Institute for Regenerative Medicine for histologic section preparation and the center for Biologic Imaging at the University of Pittsburgh for access to imaging facilities. Partial funding of this study was provided by CR Bard, Inc.

Appendix A. Supplementary data

Supplementary data to this article can be found online at https://doi.org/10.1016/j.regen.2018.12.002.

References

1. Beadles CA, Meagher AD, Charles AG. Trends in emergent hernia repair in the United States. *JAMA Surg.* 2015;150(3):194–200.
2. Beale EW, et al. The role of biologic mesh in abdominal wall reconstruction: a systematic review of the current literature. *Am J Surg.* 2012;204(4):510–517.
3. Bilsel Y, Abci I. The search for ideal hernia repair; mesh materials and types. *Int J Surg.* 2012;10(6):317–321.
4. Bellon JM, et al. Partially absorbable meshes for hernia repair offer advantages over nonabsorbable meshes. *Am J Surg.* 2007;194(1):68–74.
5. Ulrich D, et al. A preclinical evaluation of alternative synthetic biomaterials for fascial defect repair using a rat abdominal hernia model. *PLoS One.* 2012;7(11):e50044.
6. Londono R, Badylak SF. Factors wich affect the host response to biomaterials. In: Badylak SF, ed. *Host Response to Biomaterials the Impact of Host Response on Biomaterial Selection.* USA: Elsevier; 2015:1–10.
7. Brown BN, et al. Effects of age-related shifts in cellular function and local microenvironment upon the innate immune response to implants. *Semin Immunol.* 2017;29:24–32.
8. Todros S, et al. Synthetic surgical meshes used in abdominal wall surgery: Part II-Biomechanical aspects. *J Biomed Mater Res B Appl Biomater.* 2017;105(4):892–903.
9. Todros S, Pavan PG, Natali AN. Synthetic surgical meshes used in abdominal wall surgery: Part I-materials and structural conformation. *J Biomed Mater Res B Appl Biomater.* 2017;105(3):689–699.
10. Chung L, et al. Key players in the immune response to biomaterial scaffolds for regenerative medicine. *Adv Drug Deliv Rev.* 2017;114:184–192.
11. Witte MB, Barbul A. General principles of wound healing. *Surg Clin N Am.* 1997;77(3):509–528.
12. Naranjo JE, et al. Regenerative medicine: lessons from mother nature. *Regen Med.* 2016;11(8):767–775.
13. Sadtler K, et al. Design, clinical translation and immunological response of biomaterials in regenerative medicine. *Nat Rev Mater.* 2016;1(7).
14. Badylak SF, Gilbert TW. Immune response to biologic scaffold materials. *Semin Immunol.* 2008;20(2):109–116.
15. Cravedi P, et al. Regenerative immunology: the immunological reaction to biomaterials. *Transpl Int.* 2017;30(12):1199–1208.
16. Klopfleisch R, Jung F. The pathology of the foreign body reaction against biomaterials. *J Biomed Mater Res A.* 2017;105(3):927–940.
17. Wolf MT, et al. Macrophage polarization in response to ECM coated polypropylene mesh. *Biomaterials.* 2014;35(25):6838–6849.
18. Anderson J, Cramer S. Perspectives on the inflammatory, healing, and foreign body responses to biomaterials and medical devices. In: Badylak SF, ed. *Host Response to Biomaterials the Impact of Host Response on Biomaterial Selection.* USA: Elsevier; 2015:13–36.
19. Brown BN, et al. Macrophage phenotype as a predictor of constructive remodeling following the implantation of biologically derived surgical mesh materials. *Acta Biomater.* 2012;8(3):978–987.
20. Faulk DM, et al. ECM hydrogel coating mitigates the chronic inflammatory response to polypropylene mesh. *Biomaterials.* 2014;35(30):8585–8595.
21. Huber A, et al. Polypropylene-containing synthetic mesh devices in soft tissue repair: a meta-analysis. *J Biomed Mater Res B Appl Biomater.* 2012;100(1):145–154.
22. Hu Z, et al. Immunomodulatory ECM-like microspheres for accelerated bone regeneration in diabetes mellitus. *ACS Appl Mater Interfaces.* 2018;10(3):2377–2390.
23. Martin DP, Williams SF. Medical applications of poly-4-hydroxybutyrate: a strong flexible absorbable biomaterial. *Biochem Eng J.* 2003;16:97–105.
24. Williams SF, Rizk S, Martin DP. Poly-4-hydroxybutyrate (P4HB): a new generation of resorbable medical devices for tissue repair and regeneration. *Biomed Tech.* 2013;58(5):439–452.
25. Deeken CR, Matthews BD. Characterization of the mechanical strength, resorption properties, and histologic characteristics of a fully absorbable material (Poly-4-hydroxybutyrate-PHASIX mesh) in a porcine model of hernia repair. *ISRN Surg.* 2013;2013:238067.
26. Martin DP, et al. Characterization of poly-4-hydroxybutyrate mesh for hernia repair applications. *J Surg Res.* 2013;184(2):766–773.

27. Deeken CR, et al. Physicomechanical evaluation of polypropylene, polyester, and polytetrafluoroethylene meshes for inguinal hernia repair. *J Am Coll Surg.* 2011;212(1):68–79.
28. Gao Y, et al. Methodology of fibroblast and mesenchymal stem cell coating of surgical meshes: a pilot analysis. *J Biomed Mater Res B Appl Biomater.* 2014;102(4):797–805.
29. Deeken CR, Lake SP. Mechanical properties of the abdominal wall and biomaterials utilized for hernia repair. *J Mech Behav Biomed Mater.* 2017;74:411–427.
30. Cavallo JA, et al. Remodeling characteristics and biomechanical properties of a crosslinked versus a non-crosslinked porcine dermis scaffolds in a porcine model of ventral hernia repair. *Hernia.* 2015;19(2):207–218.
31. Sicari B, Turner N, Badylak SF. An in vivo model system for evaluation of the host response to biomaterials. *Methods Mol Biol.* 2013;1037:3–25.
32. Valentin JE, et al. Extracellular matrix bioscaffolds for orthopaedic applications. *J Bone Joint Surg.* 2006;88–A(12):2673–2686.
33. Sicari BM, et al. The promotion of a constructive macrophage phenotype by solubilized extracellular matrix. *Biomaterials.* 2014;35(30):8605–8612.
34. Freytes DO, et al. Preparation and rheological characterization of a gel form of the porcine urinary bladder matrix. *Biomaterials.* 2008;29(11):1630–1637.
35. Englen MD, et al. Granulocyte/macrophage colony-stimulating factor is expressed and secreted in cultures of murine L929 cells. *J Immunol Methods.* 1995;184(2):281–283.
36. Shearer JD, et al. Differential regulation of macrophage arginine metabolism: a proposed role in wound healing. *Am J Physiol.* 1997;272(2 Pt 1):E181–E190.
37. Huleihel L, et al. Macrophage phenotype in response to ECM bioscaffolds. *Semin Immunol.* 2017;29:2–13.
38. Brown BN, et al. Macrophage polarization: an opportunity for improved outcomes in biomaterials and regenerative medicine. *Biomaterials.* 2012;33(15):3792–3802.
39. Londono R, Badylak SF. Biologic scaffolds for regenerative medicine: mechanisms of in vivo remodeling. *Ann Biomed Eng.* 2015;43(3):577–592.
40. Sheikh Z, et al. Macrophages, foreign body giant cells and their response to implantable biomaterials. *Materials (Basel).* 2015;8(9):5671–5701.
41. Mantovani A, et al. The chemokine system in diverse forms of macrophage activation and polarization. *Trends Immunol.* 2004;25(12):677–686.
42. Brown BN, Sicari BM, Badylak SF. Rethinking regenerative medicine: a macrophage-centered approach. *Front Immunol.* 2014;5:510 (1-11).
43. Wynn TA. Type 2 cytokines: mechanisms and therapeutic strategies. *Nat Rev Immunol.* 2015;15(5):271–282.
44. Nucera S, Biziato D, De Palma M. The interplay between macrophages and angiogenesis in development, tissue injury and regeneration. *Int J Dev Biol.* 2011;55(4-5):495–503.
45. Haldar M, Murphy KM. Origin, development, and homeostasis of tissue-resident macrophages. *Immunol Rev.* 2014;262:25–35.
46. Wynn TA, Chawla A, Pollard JW. Macrophage biology in development, homeostasis and disease. *Nature.* 2013;496(7446):445–455.
47. Gordon S, Martinez-Pomares L. Physiological roles of macrophages. *Pflügers Archiv.* 2017;469(3-4):365–374.
48. Tidball JG, Wehling-Henricks M. Macrophages promote muscle membrane repair and muscle fibre growth and regeneration during modified muscle loading in mice in vivo. *J Physiol.* 2007;578(Pt 1):327–336.
49. Tidball JG, Villalta SA. Regulatory interactions between muscle and the immune system during muscle regeneration. *Am J Physiol Regul Integr Comp Physiol.* 2010;298(5):R1173–R1187.
50. Godwin JW, Pintoa AR, Rosenthal NA. Macrophages are required for adult salamander limb regeneration. *Proc Natl Acad Sci Unit States Am.* 2013;110(23):9415–9420.
51. Wynn TA, Vannella KM. Macrophages in tissue repair, regeneration, and fibrosis. *Immunity.* 2016;44(3):450–462.
52. Vannella KM, Wynn TA. Mechanisms of organ injury and repair by macrophages. *Annu Rev Physiol.* 2017;79:593–617.
53. Jacobsen G, DuCoin C. Biodegradable meshes in abdominal wall surgery. In: Novitsky YW, ed. *Hernia Surgery: Current Principles.* Switzerland: Springer International Publishing; 2016:71–78.
54. Hjort H, et al. Three-year results from a preclinical implantation study of a long-term resorbable surgical mesh with time-dependent mechanical characteristics. *Hernia.* 2012;16(2):191–197.
55. Pascual G, et al. Repair of abdominal wall defects with biodegradable laminar prostheses: polymeric or biological? *PLoS One.* 2012;7(12):e52628.
56. Amid PK. Classification of biomaterials and their related complications in abdominal wall hernia surgery. *Hernia.* 1997;1(1):15–21.
57. Kalaba S, et al. Design strategies and applications of biomaterials and devices for hernia repair. *Bioact Mater.* 2016;1(1):2–17.
58. Ruiz-Jasbon F, et al. Inguinal hernia repair using a synthetic long-term resorbable mesh: results from a 3-year prospective safety and performance study. *Hernia.* 2014;18(5):723–730.
59. Peeters E, et al. One-year outcome of biological and synthetic bioabsorbable meshes for augmentation of large abdominal wall defects in a rabbit model. *J Surg Res.* 2013;180(2):274–283.
60. Reing JE, et al. The effects of processing methods upon mechanical and biologic properties of porcine dermal extracellular matrix scaffolds. *Biomaterials.* 2010;31(33):8626–8633.
61. Sun WQ, et al. Process-induced extracellular matrix alterations affect the mechanisms of soft tissue repair and regeneration. *J Tissue Eng.* 2013;4 p. 2041731413505305.
62. Bryan N, et al. The in vivo evaluation of tissue-based biomaterials in a rat full-thickness abdominal wall defect model. *J Biomed Mater Res B Appl Biomater.* 2014;102(4):709–720.
63. Donohoe DR, et al. The Warburg effect dictates the mechanism of butyrate-mediated histone acetylation and cell proliferation. *Mol Cell.* 2012;48(4):612–626.
64. Russo I, et al. Butyrate attenuates lipopolysaccharide-induced inflammation in intestinal cells and Crohn's mucosa through modulation of antioxidant defense machinery. *PLoS One.* 2012;7(3):e32841.
65. Nelson T, et al. The extraneural distribution of g-hydroxybutyrate. *J Neurochem.* 1981;37(5):1345–1348.
66. Mamelak M. Alzheimer' s disease, oxidative stress and gammahydroxybutyrate. *Neurobiol Aging.* 2007;28(9):1340–1360.
67. Gall WE, et al. alpha-hydroxybutyrate is an early biomarker of insulin resistance and glucose intolerance in a nondiabetic population. *PLoS One.* 2010;5(5):e10883.
68. Owen OE, et al. Brain metabolism during fasting. *J Clin Invest.* 1967;46(10):1589–1595.
69. Roth JS, et al. Prospective evaluation of poly-4-hydroxybutyrate mesh in CDC class I/high-risk ventral and incisional hernia repair: 18-month follow-up. *Surg Endosc.* 2018;32(4):1929–1936.
70. Anderson J. Foreword. *Host Response to Biomaterials: The Impact of Host Response on Biomaterial Selection.* Academic Press; 2015 p. xiii.
71. Sadtler K, et al. Developing a pro-regenerative biomaterial scaffold microenvironment requires T helper 2 cells. *Science.* 2016;352(6283):366–370.
72. Tan J, et al. The role of short-chain fatty acids in health and disease. *Adv Immunol.* 2014;121:91–119.